

Nanoscale

Accepted Manuscript



This is an *Accepted Manuscript*, which has been through the Royal Society of Chemistry peer review process and has been accepted for publication.

Accepted Manuscripts are published online shortly after acceptance, before technical editing, formatting and proof reading. Using this free service, authors can make their results available to the community, in citable form, before we publish the edited article. We will replace this *Accepted Manuscript* with the edited and formatted *Advance Article* as soon as it is available.

You can find more information about *Accepted Manuscripts* in the [Information for Authors](#).

Please note that technical editing may introduce minor changes to the text and/or graphics, which may alter content. The journal's standard [Terms & Conditions](#) and the [Ethical guidelines](#) still apply. In no event shall the Royal Society of Chemistry be held responsible for any errors or omissions in this *Accepted Manuscript* or any consequences arising from the use of any information it contains.



Progress Toward Clonable Inorganic Nanoparticles

Thomas W. Ni^{a,†}, Lucian C. Staicu^{a,2,††}, Richard S. Nemeth^{a,†}, Cindi Schwartz^{3,††},
David Crawford^a, Jeffrey D. Seligman^a, William J. Hunter⁴, Elizabeth Pilon-
Smits², Christopher J. Ackerson^a

Received 00th January 20xx,
Accepted 00th January 20xx

DOI: 10.1039/x0xx00000x

www.rsc.org/

Pseudomonas moraviensis stanleyae was recently isolated from the roots of the Selenium (Se) hyperaccumulator plant *Stanleya pinnata*. This bacterium tolerates normally lethal concentrations of SeO_3^{2-} in liquid culture, where it also produces Se nanoparticles. Structure and cellular ultrastructure of the Se nanoparticles as determined by cellular electron tomography shows the nanoparticles as intracellular, of narrow dispersity, symmetrically irregular and without any observable membrane or structured protein shell. Protein mass spectrometry of a fractionated soluble cytosolic material with selenite reducing capability identified nitrite reductase and glutathione reductase homologues as NADPH dependent candidate enzymes for the reduction of selenite to zerovalent Se nanoparticles. *In vitro* experiments with commercially sourced glutathione reductase revealed that the enzyme can reduce SeO_3^{2-} (selenite) to Se nanoparticles in an NADPH-dependent process. The disappearance of the enzyme as determined by protein assay during nanoparticle formation suggests that glutathione reductase is associated with or possibly entombed in the nanoparticles whose formation it catalyzes. Chemically dissolving the nanoparticles releases the enzyme. The size of the nanoparticles varies with SeO_3^{2-} concentration, varying in size from 5 nm diameter when formed at 1.0 μM [SeO_3^{2-}] to 50 nm maximum diameter when formed at 100 μM [SeO_3^{2-}]. In aggregate, we suggest that glutathione reductase possesses the key attributes of a clonable nanoparticle system: ion reduction, nanoparticle retention and size control of the nanoparticle at the enzyme site.

1 Introduction

A *grand challenge* in biogenic inorganic nanoparticle synthesis is a clonable nanoparticle. That is, specifically, a *single* clonable polypeptide sequence that mediates the self-contained formation of an inorganic nanoparticle from inorganic salt precursors. Just as the clonable fluorophore, green fluorescent protein (GFP), is widely used for clonable contrast in biological optical microscopies,¹ a clonable inorganic and electron-dense nanoparticle is expected to find widespread use for cellular contrast in biological electron microscopy. In each case facile genetic methods for concatenating DNA encoding a protein sequence to the DNA sequence of a native cellular protein underlie the utility of clonable microscopy contrast. Expression of the resulting chimeric protein places a contrast marker alongside every instance of the native protein, enabling localization of the

protein chimera in micrographs.

A clonable nanoparticle requires a polypeptide that integrates three distinct chemical activities. One activity is inorganic ion reduction or oxidation, converting soluble (ideally bioavailable and nontoxic) inorganic ions to insoluble (nanoparticulate) species. Second, the resulting inorganic nanoparticle must be retained by the polypeptide. Third, the size of the resulting nanoparticle must be large enough to identify unambiguously in a micrograph that includes biological structure, while also being small enough to minimize perturbation of cell biology and to reduce the shadow-casting that obscures biological information. An ideal size is suggested as 5 nm diameter, as this size is considered to allow unambiguous identification of particles over cellular background. Smaller sizes may be useful for more specialized applications. So far, there is no widely adopted clonable contrast marker in biological electron microscopy.

Both naturally occurring proteins as well as peptides isolated from libraries are investigated as candidate clonable nanoparticles. Naturally occurring proteins investigated include most prominently ferritin and metallothionein. In the case of the iron-storage capsule protein ferritin,² the requirement of 24 subunits with a total mass of nearly 0.45 MDa³ may limit its use. Metallothionein coordination of Au(I)

^a Department of Chemistry, Colorado State University, Fort Collins, CO 80523, USA.

^b Address here.

^c Address here.

† Footnotes relating to the title and/or authors should appear here.

Electronic Supplementary Information (ESI) available: [details of any supplementary information available should be included here]. See DOI: 10.1039/x0xx00000x

or Au(III) based ions is also proposed,⁴⁻⁶ but these methods are not widely adopted in biological electron microscopy. This is perhaps because the Au(I) precursors are sparingly soluble in water and Au(III)-based coordination compound precursors are easily reduced by proteins,⁷⁻⁹ buffers,^{10,11} and other biomolecules encountered in a cellular environment.¹²⁻¹⁵

Proteins associated with magnetosomes such as mms6 are also initially attractive for forming clonable iron oxides.¹⁶ However, a recent study shows that cloning of a minimal set of magnetosome-associated genes into a new host cell results in membrane-encapsulated iron oxide nanoparticles.¹⁷ Such a membrane would clearly disrupt the function of a clonable nanoparticle, by adding size and possibly membrane sequestering proteins tagged for study.

Another investigated source of a polypeptide satisfying the clonable nanoparticle criteria is directed evolution. Directed evolution methods have already identified several DNAs,¹⁸⁻²⁰ RNAs,^{21,22} and peptides²³⁻²⁵ that mediate inorganic nanoparticle formation. In fact, early reports suggested that some library-derived peptides possessed the three desired activities of reduction, retention and size control.^{23,26} Subsequent studies revealed that the buffers such as HEPES¹¹ or other Good's Buffers,¹⁰ in which the selections were executed, reduced the inorganic precursors.²⁷ The role of the evolved biomolecules is to cap the nanoparticles resulting from buffer reduction of metal ions, enforcing size and shape control. One of the best studied systems, the A3 peptide,^{26,28-31} shows a preference for a size where the radius of curvature of the nanoparticle matches the curvature naturally adopted by the peptide.²⁸ Thus, while inorganic nanoparticle binding (retention) and size control are now well-established for peptides and polynucleotides, there are no well-established examples of peptides that catalytically or stoichiometrically reduce metal ions for the production of particles large enough to find use in biological electron microscopy.

Enzymes that reduce or oxidize metal ions into insoluble forms represent another class of biomolecule candidate for a clonable nanoparticle, and are the least extensively investigated. Such enzymes include silicateins,^{32,33} silicatein homologous proteases,³⁴ and metal^{35,36} and metalloid³⁷⁻³⁹ reductases implicated in detoxification processes. Resulting nanoparticle size is regulated when the product is retained, by encapsulating proteins such as DPS⁴⁰ or ferritin.⁴⁰ Alternatively, enzymes release or turn over their products, allowing them to diffuse from the site of synthesis.^{34,41} Notably, there are no well-established examples of intracellular particles wherein the inorganic portion of the particle is exposed to cytosol.

In the present work, we investigate the formation, enzymology, structure and cellular ultrastructure of biogenic selenium nanoparticles (SeNPs) made by a strain of *Pseudomonas fluorescens*, *P. moraviensis* Stanleyae, recently isolated from a seleniferous environment, inside Se hyperaccumulator plant *Stanleya pinnata*. While Se is an essential element for many organisms, the range between essentiality and toxicity is very narrow.⁴² The conversion of comparatively toxic Se oxyanions, SeO₃²⁻ (selenite) and SeO₄²⁻

(selenate) to zerovalent SeNPs by selenospecialist bacteria has been previously established.^{38,39,43,44} Depending on the species, the resulting SeNPs may be extra- or intra-cellular.⁴⁵ Enzymes including nitrite reductase, thioredoxin, glutathione reductase, and metalloid reductases are identified by proteomic mass spectrometry on purified nanoparticles or in fractionated cell extracts assayed for Se oxyanion reductase activity.³⁷⁻³⁹ Very little is known about the mechanism of particle synthesis, the relationship between enzymes that synthesize the nanoparticles and the nanoparticles, and the physical interface between nanoparticles and the cytosol. For instance, most intracellular nanoparticles are coated by a membrane or a structured protein coat. There is also little investigation of the means of size control for biogenic and/or enzymatically produced Se nanoparticles.

In the present work, we report the first 3D electron tomographic reconstructions of cells containing SeNPs, and infer unprecedented aspects of the nanoparticle and nanoparticle/cytosol interface that may be unique to SeNPs, and especially relevant for the application of SeNPs as a clonable nanoparticle. We show the possibility of size control of the nanoparticles, and show that a large fraction of enzymes are physically associated with nanoparticles. Overall, our results present the first report of a polypeptide that possesses the three coincident activities required for a clonable nanoparticle useful in cellular electron microscopy: precursor reduction, product retention, and product size-control.

2 Results

Pseudomonas moraviensis stanleyae was isolated from the roots of *Stanleya pinnata*, a Se hyperaccumulator plant native to western USA,⁴⁶ and observed to tolerate unusually high concentrations of SeO₃²⁻. When grown in Luria Broth media supplemented with 10 mM Na₂SeO₃, the cultures become notably pink in color during early log-phase. This color change (Figure S1) is associated with the formation of zerovalent (red) Se. The conversion of selenite oxyanions to zerovalent Se is a common detoxification process for bacteria that tolerate high concentrations of Se oxyanions.⁴⁷ Initial characterization of the SeNPs produced by *P.*

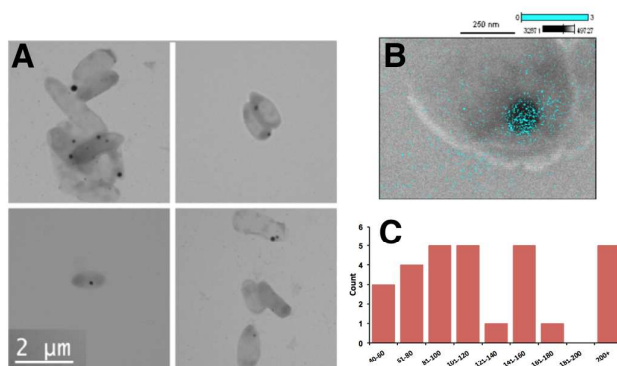


Figure 1. Transmission electron micrographs of glutaraldehyde-fixed dry mounted cells are shown in panel A. Electron-dense (dark) inclusions are present in many of the cells of panel A, as well as outside the cells. Panel B shows a scanning transmission micrograph of a selected area of one of the cells that includes a dark inclusion; overlaid on this inclusion is an EDS map of Se in the sample, indicating the presence of Se in the sample. Panel C shows the distribution of observed particle sizes.

moraviensis Stanleyae was performed by transmission electron microscopy (TEM), scanning electron microscopy (SEM) with energy dispersive X-Ray spectroscopy (EDS) elemental mapping, and 3-D cellular electron tomography.

An initial TEM examination of glutaraldehyde-fixed concentrated cell culture of *P. moraviensis* Stanleyae, dry mounted on a carbon-coated TEM grid (Figure 1, left panel) revealed relatively uniform (107 ± 35 nm) high-contrast circular morphology spots both inside (or superimposed on) and outside of the bacterial cells. Scanning transmission electron microscopy of the same sample allowed EDS mapping

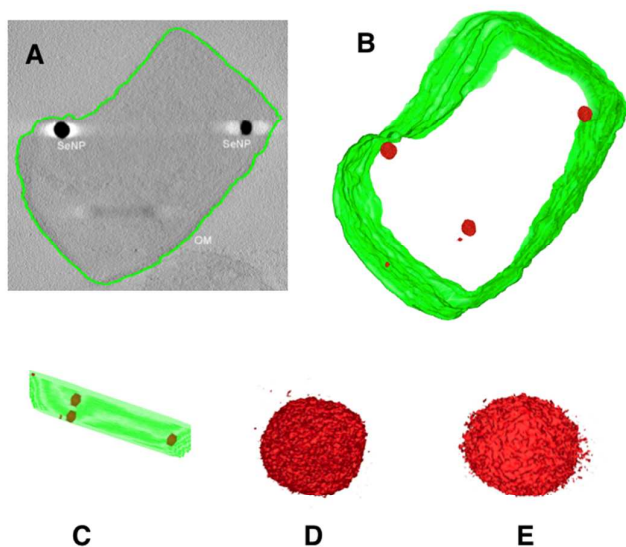


Figure 2. Electron tomographic reconstruction of *P. moraviensis* Stanleyae. The reconstruction was segmented to reveal the outer membrane and SeNP nanoparticles (panels A, B, and C.) Magnified views of two SeNPs are shown in panels D and E; Panel D shows the large SeNP in the middle of the cell in panel B. Panel E shows the large SeNP in the upper left part of the cell in panel B. The full (unsegmented) reconstruction is available as supporting information in IMOD

of elemental composition. The EDS mapping confirms that the high-contrast spots are Se-rich. (Figure 1, panel B) This suggests that the high-contrast spots are Se nanoparticles that account for the red color of the bacterial cultures. A histogram of particles sizes is shown in Figure 1, panel C. Similar spots were not observed in TEM images control cultures that were not supplemented with SeO_3^{2-} . At least 50 were examined in the control observation, high density spots were observed associated only with one cell, and in that instance the morphology was notably irregular compared to the putative SeNPs (Figure S2.)

Dry mount electron microscopy provides comparatively limited information compared to more sophisticated preservation and imaging methods, such as cellular electron tomography.^{48,49} With appropriate preservation,⁵⁰⁻⁵² these methods allow high fidelity 3D resolution of cellular ultrastructure such as membranes and major cytoskeletal filaments, organelles and ribosomes.⁵³ Here we used electron tomography to definitively reveal whether the observed nanoparticles are inside the cells

(as opposed to superimposed), reveal membranes, and reveal major cellular ultrastructure. *P. moraviensis* Stanleyae cells were grown as described in the methods section, both with and without 10 mM SeO_3^{2-} supplementation into the stationary phase where particles are easily discernable. Concentrated cultures were subjected to freeze substitution,⁵⁰ which provides the highest fidelity preservation of cellular ultrastructure aside from vitrification.⁵⁴ Vitrification was not used here because the size of the cells (400-600 nm in the minimum dimension) would require cryo-sectioning, which is technically difficult.

Three tomographic tilt-series were acquired of both SeO_3^{2-} and control samples at 6, 9, 12, and 36 hours after addition of SeO_3^{2-} or an equivalent volume of media. The spherical inclusions we attribute to SeNPs were not present in any of the tilt series recorded of cells that were not supplemented with SeO_3^{2-} . The spherical inclusions were most abundant in cells grown in the presence of SeO_3^{2-} for 36 hours, with media replaced every 12 hours to maintain cell health as described in the methods.

3D reconstructions of both unstained and osmium stained 200 nm sections revealed large inclusions inside the SeO_3^{2-} supplemented cells. In the case of metal-stained cells, it was unclear whether the inclusions could be attributed to the staining of biological material or to SeNPs, although other ultrastructures (such as both inner and outer membranes) were clearly revealed (Figure S3).

The reconstructions of unstained cells were more informative. Two of the tilt series containing putative SeNPs were reconstructed and segmented. Figure 2 shows a segmented reconstruction of a single cell; the outer membrane was segmented by hand, as is current standard practice with IMOD, while the SeNPs were sufficiently electron dense that segmentation could be accomplished automatically with a simple thresholding operation. Imodauto was set at a threshold of 1 (out of 255), which generated a model. This clearly auto-segments out high-density inclusions that we attributed to SeNPs. In each of three 3D reconstructions of cells grown with SeO_3^{2-} supplementation we observed high-contrast inclusions of 58.66 ± 2.47 nm diameter (from a total of 3 particles observed).

Figure 2 shows a 3D segmentation of one of the cells, with a XY view shown in panel A and a YZ view shown in panel B. These two views reveal unambiguously for the first time that large SeNPs can be intracellularly contained, where previous studies were 2D microscopy and could not rule out that particles and cells are superimposed. Notably, there is no evidence that these particles are membrane-encapsulated, as is observed for other inorganic inclusions such as magnetosomes.⁵⁵

Panels D and E of Figure 2 show the three larger intracellular particles at greater magnification. From these images it appears that while the particles are “approximately spherical” they are not perfectly spherical and in fact are symmetrically irregular. Some of the irregularity in these images is artifact. The “spikiness / texture” of the surface is also observed for the 10 nm diameter gold nanoparticles used as fiducial markers for alignment.⁵² The anisotropic ‘speckling’ halo that surrounds

some of the particles likely arises from the 'missing wedge' artifact in electron tomography.⁵⁶ Even accounting for these sources of artifact, however, the nanoparticles appear symmetrically irregular.

To derive greater insight into the mechanism of formation of these SeNPs, we identified proteins implicated in the reduction of SeO_3^{2-} to $\text{Se}(0)$ by *P. moraviensis* stanleyae. Briefly we fractionated the soluble proteins from cell lysate on a nondenaturing polyacrylamide gel, and then stained the gel with metalloids oxyanions and electron donating cofactors. Any resulting bands indicating the presence of NADPH-dependent selenite reductase activity were excised and further analyzed by proteomic mass spectrometry.

To obtain better resolution, cell lysate of *P. moraviensis* Stanleyae grown in SeO_3^{2-} -supplemented media was further fractionated on a hydrophobic interaction column (HIC) that was eluted with different concentrations of $(\text{NH}_4)_2\text{SO}_4$. Proteins in each fraction from the HIC column were separated on a non-denaturing polyacrylamide gel. To develop bands corresponding to selenite reductases, gels were placed into nitrogen-filled zip-lock bags filled with a buffer supplemented with metalloids oxyanions and NADPH or NADH. The entire protocol was adapted from previous work by Hunter.³⁸

Figure 3 shows the results of this experiment for the reduction of SeO_3^{2-} in the presence of NADPH. Clearly there are proteins with selenite reductase activity present in some of the HIC fractions. No notable reduction of selenate or tellurate (TeO_4^{2-}) to elemental form was noted, and the reduction of SeO_3^{2-} and TeO_3^{2-} was notably weaker when NADH instead of NADPH was used as an electron donor. No bands developed in the absence of NADH or NADPH.

Figure 3 shows that two bands develop in the anaerobic SeO_3^{2-} + NADPH incubation condition, one that is associated with lower salt elutions from the HIC column and a second associated with higher salt elutions.

To identify the proteins involved in the observed reduction, we excised the bands and identified associated proteins by protein mass spectrometry. From a total of 5 activity bands excised and analyzed for protein content, 122 proteins were identified (Table S1). Of these proteins 7 are known to be NADPH or NADP^+ dependent. This set of NADPH-dependent proteins (Table 1) comprises a set of candidate proteins for specific NADPH-dependent SeO_3^{2-} reduction to $\text{Se}(0)$.

Of these proteins, we were especially interested in glutathione reductase (GSHR) and nitrite reductase, as each was previously implicated in selenite reduction.^{38,57-59} To validate the specificity and investigate the enzymatic mechanism, we obtained baker's yeast (*Saccharomyces cerevisiae*) GSHR from Sigma-Aldrich (G3664) and the NADPH-dependent cytochrome C reductase (C3381) and *Aspergillus niger* nitrate reductase

(N7265) as comparison control enzymes. Each enzyme was tested for competence to reduce SeO_4^{2-} , SeO_3^{2-} , TeO_4^{2-} , and TeO_3^{2-} to zerovalent forms of Se and Te, respectively, as judged by a color change of the solution from clear to turbid red (Se) or gray (Te) upon inclusion of either NADH or NADPH as electron donors. In this initial screening of enzymes and substrate specificity, we found that GSHR with NADPH as an electron donor could reduce SeO_3^{2-} and TeO_3^{2-} , while no other combination resulted in notable metalloid oxyanion reduction. In order to understand the mechanism by which GSHR converts these metalloid oxyanions, we first characterized basic enzymatic properties for both SeO_3^{2-} and TeO_3^{2-} substrates. K_m and V_{max} were determined by observing the rate of consumption of NADPH, which has an easily observable spectroscopic signature (Figure S4). We found a K_M of 31 mM for SeO_3^{2-} and a K_M of 0.54 mM for TeO_3^{2-} (Figure S5). The reported K_m value of GSHR for GS-SG is $\sim 50 \mu\text{M}$ ⁶⁰ suggesting that the enzyme has a substantially higher substrate affinity for GS-SG than for SeO_3^{2-} .

After dialysis to remove small molecules, the products of GSHR reduction of TeO_3^{2-} and SeO_3^{2-} were examined by TEM. Reduction of TeO_3^{2-} to $\text{Te}(0)$ by GSHR produced networks of sub 5 nm particles, where the diameters are difficult to discern, similar to the previously reported enzymatic reduction of Ti^{3+} (as TiBALD) by cysteine and serine proteases.^[34] Reduction of SeO_3^{2-} to $\text{Se}(0)$ in otherwise identical conditions resulted in larger, discrete 61 ± 37 nm diameter SeNPs. Figure 4 shows electron micrographs of each product and a histogram of size distribution for the SeNP.

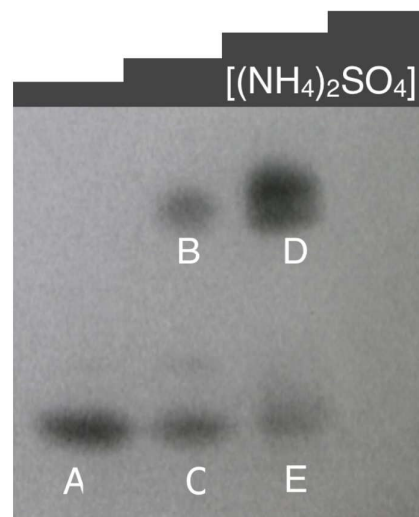


Figure 3. Native gel of HIC column fractions, stained with SeO_3^{2-} and NADPH to reveal bands containing enzymatic SeO_3^{2-} reductase activity. Lanes in the gel correspond to step fractions taken from a HIC column to process crude cell lysate. Lanes correspond to 0.1 M, 0.5M, 1.0M, 1.5M and 2.0M elutions of the HIC column with $(\text{NH}_4)_2\text{SO}_4$.

| Oxyreductase | Accension Number | MW (Da) | Cofactor/Rxn | Band Association |
|--|------------------|---------|-------------------------------------|------------------|
| Nitrite and Sulfite Reductase | gi 77459334 | 62,262 | NADPH | B |
| Isocitrate dehydrogenase [Pseudomonas fluorescens SBW25] | gi 229591243 | 66,003 | NADP ⁺ /ATP | B, C, D |
| Glutathione Reductase [Pseudomonas fluorescens Pf0-1] | gi 77459153 | 49,244 | NADP ⁺ /FAD | B, D |
| 5,10-methylenetetrahydrofolate reductase [Pseudomonas fluorescens Pf0-1] | gi 77461502 | 31,515 | NADP ⁺ /FAD | B, D |
| 3-ketoacyl-ACP reductase [Pseudomonas fluorescens Pf0-1] | gi 77460378 | 25,500 | NADPH | A |
| Thiol Peroxidase [Pseudomonas fluorescens Pf0-1] | gi 77458745 | 17,586 | NADPH/H ₂ O ₂ | B, D |
| 4-aminobutyrate aminotransferase [Pseudomonas fluorescens Pf0-1] | gi 77456416 | 44,837 | NADPH | A, B, C, D, E |

Table 1. NADPH-dependent enzymes identified in mass spectrometry

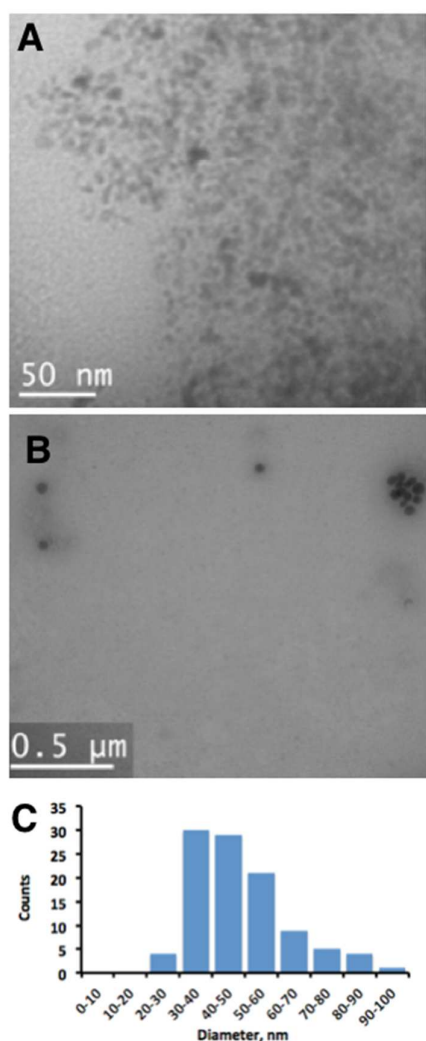


Figure 4. Transmission electron micrographs of the characterization of *in vitro* products of GSHR reduction of TeO_3^{2-} (panel A) and SeO_3^{2-} (panel B). Panel C shows the size distribution histogram observed for GSHR produced SeNPs.

In the enzymatic assays, we observed that the steady-state phase of product production was remarkably short-lived (Figure S5). We subsequently observed that the enzyme itself was consumed in the *in vitro* reaction, as determined by a Bradford assay for total protein (Figure 5, circles). This suggested that the enzyme is associated with the particles it synthesizes, perhaps even entombed in the particle. To test this hypothesis of association or entombment, we separated by centrifugation the enzymatically formed SeNPs from soluble enzyme. The insoluble protein fraction corresponded to 18% of the total enzyme in the assay. SeNPs are known to be dissolvable in solvents such as ethylenediamine and benzene.⁶¹ We found that enzymatically produced SeNPs are also soluble in Bradford protein assay. In fact, we could recover nearly quantitatively the protein that disappears from the enzymatic assay in a Bradford assay of the enzymatically produced SeNPs. This data is shown in Figure 5, upper left panel. There is evidence that the soluble fraction of GSHR is also associated with smaller SeNPs. In an SDS-PAGE of the soluble fraction of GSHR, a difference in electrophoretic mobility coupled to a

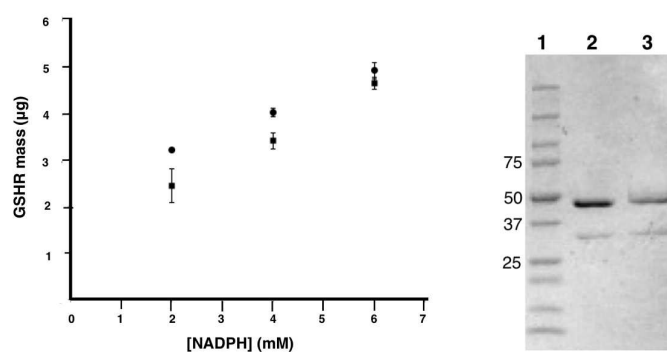


Figure 5. Left panel shows the amount of GSHR lost from the assay at different NADPH cofactor concentrations in circles. In squares is depicted the amount of protein measured from the insoluble selenium particles created during the assay. The agreement between protein lost from the assay and protein recovered from the particles suggests that the enzyme is associated or entombed in the particles it creates. The right panel shows an SDS-PAGE of the soluble fraction of GSHR after an assay. The small shift in electrophoretic mobility and large smear above the band can be attributed to association between the enzyme and smaller SeNPs.

'smearing of the band', consistent with the enzyme being bound to polydisperse particles, is observed in comparison to a control reaction (Figure 5, right panel). Overall, we suggest that some fraction of the enzyme is associated with or entombed in the nanoparticles that the enzyme creates. When NADPH cofactor is omitted from the reaction, the enzymatic process does not proceed, and the observed enzyme concentration remains constant (Figure S6 top panel, diamonds).

The size of the enzymatically synthesized SeNPs is controllable through modulation of enzyme substrate concentrations. By varying the [NADPH] in an *in vivo* reaction, we observed that we could vary the size of the resulting particles from 2.5 nm to more than 50 nm diameter. The effect of [NADPH] on particle size is shown in Figure S7.

3 Discussion

We identify the first polypeptide capable of soluble precursor reduction, retention of reduced product at the site of reduction, and size control of the reduced product. This represents a notable step in progress toward a clonable nanoparticle, which is fundamentally different from other proposed strategies for clonable nanoparticles. First, other strategies rely on stoichiometric binding of metal ions,^{4,5} or on oxidation events,² while this approach uses enzymes and NADPH as an electron donor to reduce inorganic precursors. We infer that the products of reduction are often retained by the enzyme that creates them, possibly by an entombing mechanism. This rare combination of three activities in biogenic nanoparticle production was previously suggested for reduction of Au(III) precursors by the same enzyme.³⁵ In that work, however, the resulting particles are quite small, and as noted above, Au reduction is quite promiscuous by biomolecules, (8) while the selenite and tellurite reductions reported here appear specific to just a handful of enzymes, as evidenced by Figure 3.

We observe notable differences in the resulting size of particles, depending on the growth condition. We cultured *P. moraviensis* Stanleyae cells for up to 36 hours in the presence of SeO_3^{2-} supplementation, to ensure an abundance of SeNPs in subsequent microscopic examination. We grew cells for this extended time both with and without replacement of media. When the media was not replaced, it is likely that it is depleted of necessary nutrients at the 36 hour time point, and the cells are starving. The starvation condition of cells in Figures 1 and S2 may partially explain the difference in average particle size observed between the intracellular particles in Figure 1 (107 nm diameter) and Figure 2 (58 nm diameter). Notably, in Figure S3 the membranes are quite distorted, consistent with starving cells that are having difficulty maintaining homeostasis. The starvation condition was avoided for cells reconstructed for Figure 2 by replacing the growth media every 12 hours. Note that particle diameters measured for SeNPs in 'healthy' cells (58 nm diameter average diameter) and SeNPs produced *in vitro* by GSHR (61 nm average diameter) are within measurement error. This concurrence in

particle size suggests that the *in vitro* and *in vivo* mechanisms that underlie the formation of these SeNPs are similar.

Key for future application is minimizing the mass of the biological components of clonable nanoparticles. For instance, the mass of GFP is 27 kDa, yet some studies have demonstrated that GFP concatemers can interrupt the native function of the protein fused to GFP.^{61,62} A finding we make relevant to minimizing the mass of clonable nanoparticle tags is that the SeNPs described here may be effectively naked. This stands in contrast to the well-established intracellular inorganic nanoparticles, which are coated either by a membrane or by a structured protein capsule.

We hypothesize that the particles are naked, with the Se(0) exposed to the cytosol, from a combination of structural and chemical evidence. From the tomographic reconstructions, we observe no evidence for a membrane around the SeNPs, while membranes are easily observed for naturally occurring magnetite nanoparticles.⁵⁵ The low symmetry of the particles, dispersity, and differences in average size that depend on growth conditions suggest that there is no structured protein coat, such as that found with ferritin and DPS-coated nanoparticles.

Chemically, we note that nearly all clusters and nanoparticles require a ligand shell to quench the chemical reactivity associated with the open valence electron shells of most pure elements. A handful of elements, however, including Se and Te as well as As, Bi, and Sb are known to form stable naked cluster compounds.⁶³

This is in many cases because the element can achieve noble gas-like electron counts by catenation, often resulting in ring structures in the solid state, such as the well-known S_n , Se_n , and Te_n ring compounds where $6 \leq n \leq 8$. Indeed, a recent report suggests that while the surface of SeNPs is more complex than an approximately scaled giant naked Se cluster, the surfaces are stable without formal ligation.⁶⁴ Furthermore, protein mass spectrometry on purified SeNPs fails to identify candidate proteins that are known to interact with inorganic ions or surfaces.³⁷ Thus, the combination of irregular symmetry, absence of a membrane, and plausibility of a ligand-free surface suggests that SeNPs may represent the first described class of cytosol exposed inorganic nanoparticle surfaces.

The commercially sourced GSHR and GSHR or GSHR-like enzymes identified in *P. moraviensis* Stanleyae are not immediately useful as a clonable label in cellular EM. First, the resulting SeNPs are substantially larger than practical; second, other GSHRs, nitrite reductases, and thioredoxin⁶⁵ may also produce background particles. While these enzymes are not characterized *in vitro* as producing SeNPs, they are characterized as using SeO_3^{2-} as a substrate. We have not yet evaluated the portability of this clonable nanoparticle for use in other cell lines. The concentrations of SeO_3^{2-} we used in both the *in vitro* and *in vivo* work herein are in the range where toxicity is expected for most cells and organisms. The K_M of the baker's yeast enzyme is low, especially compared to oxidized GS-SG and GS-Se-SG substrates investigated historically for this enzyme.^{60,66} Due to the measured K_M , the

baker's yeast GSHR will always require typically toxic concentrations of SeO_3^{2-} for nanoparticle formation. Furthermore, specialized selenium transporters that may be present in the selenium hyperaccumulator studied here may also enable the large intracellular particles observed in Figures 1 and 2. Thus, we anticipate cloning the GSHR-like enzyme from *P. moraviensis* Stanleyae, under the hypothesis that this selenium-specialized enzyme will have a much more favorable K_M , and that the enzyme may function well with physiologically normal concentrations of SeO_3^{2-} while simultaneously conferring resistance to Se toxicity to cells in which it is expressed. An enzyme optimized for selenite or tellurite reduction may allow superior labeling specificity by kinetically outrunning any competing reactions.

While additional work is required to complete the adaptation of this clonable nanoparticle approach for general cellular use, this approach may find more immediate use in labeling purified macromolecular complexes. Presently labeling with *ex situ* synthesized gold nanoparticles is state-of-the-art for this purpose, with applications in molecular EM, X-ray free-electron laser, and SAXS studies of macromolecular complexes.⁶⁷ A clonable approach to this contrast problem may make this sort of tagging much more facile.

For instance, Se (and Te) oxyanions have notable advantages as precursors over previously investigated Au and Fe-based systems. The Au(I) and Au(III) coordination compounds are broadly cross-reactive (i.e., easily reduced into background particulate material) by a wide swath of biomolecules and buffers.^{8,10,11} This broad cross-reactivity may explain the dearth of followup to reports of metallothionein / Au combinations as molecular and cellular EM labels. In contrast, the present work and some preceding work suggest that the palette of proteins that possess notable reactivity against the metalloid oxyanions TeO_3^{2-} and SeO_3^{2-} is comparatively limited in number.

Improved size control may be imposed by concatenated or co-expressed peptides. Several dodecapeptides are now known to impose size control²⁸ on a number of *in vitro* synthesized metal nanoparticles.⁶⁸ Similar peptides may be isolated to impose size control on SeNPs or TeNPs.

4 Conclusion

In conclusion, we identify the first polypeptide that appears capable of synthesizing, retaining and size-controlling an inorganic nanoparticle. By virtue of their metalloid composition, the particles may be naked and exposed to free cytosol. We also find that metalloid oxyanions are comparatively selective in their cross-reactivity against biological molecules. Overall, we suggest that metalloid reductases, including the GSHR-like reductase characterized here, comprise a class of enzymes that may find use in imaging applications needing a clonable nanoparticle.

Acknowledgements

Electron tomography was performed in the Boulder Laboratory for 3D Electron Microscopy of Cells, supported by P41GM103431 from the National Institute of General Medical Sciences to A. Hoenger. CJA acknowledges support from NIH 5 R21 EB014520. LS recognizes support from the Fulbright Commission. The manuscript was written through contributions of all authors. All authors have given approval to the final version of the manuscript. ‡These authors contributed equally.

Notes and references

- B. N. G. Giepmans, S. R. Adams, M. H. Ellisman, R. Y. Tsien, *Science*. **2006**, *312*, 217–224.
- Q. Wang, C. P. Mercogliano, J. Löwe, *Structure*. **2011**, *19*, 147–154.
- E. C. Theil, *Annu. Rev. Biochem.* **1987**, *56*, 289–315.
- C. P. Mercogliano, D. J. DeRosier, *J. Mol. Biol.* **2006**, *355*, 211–223.
- C. P. Mercogliano, D. J. DeRosier, *J. Struct. Biol.* **2007**, *160*, 70–82.
- E. Diestra, J. Fontana, P. Guichard, S. Marco, C. Risco, *J. Struct. Biol.* **2009**, *165*, 157–168.
- A. Baksi, P. L. Xavier, K. Chaudhari, N. Goswami, S. K. Pal, T. Pradeep, *Nanoscale*. **2013**, *5*, 2009–2016.
- P. L. Xavier, K. Chaudhari, A. Baksi, T. Pradeep, *Nano Rev.* **2012**, *3*.
- K. Chaudhari, P. L. Xavier, T. Pradeep, *ACS Nano* **2011**, *5*, 8816–8827.
- A. Habib, M. Tabata, Y. Wu, *Bull. Chem. Soc. Jpn.* **2005**, *78*, 262–269.
- J. Xie, J. Y. Lee, D.I.C. Wang, *Chem. Mater.* **2007**, *19*, 2823–2830.
- J. Turkevitch, *Discuss. Faraday Soc.* **1951**, *11*, 55–75.
- G. Frens, *Nature: Physical Science* **1973**, *241*, 20–22.
- J. M. de la Fuente, S. Penadés, *Biochim. Biophys. Acta.* **2006**, *1760*, 636–651.
- H. Huang, X. Yang, *Carbohydr. Res.* **2004**, *339*, 2627–2631.
- Y. Amemiya, A. Arakaki, S.S. Staniland, T. Tanaka, T. Matsunaga, *Biomaterials.* **2007**, *28*, 5381–5389.
- I. Kolinko, A. Lohße, S. Borg, O. Raschdorf, C. Jögler, Q. Tu, M. Pósfai, E. Tompa, J. M. Plitzko, A. Brachmann, G. Wanner, R. Müller, Y. Zhang, D. Schüler, *Nat. Nanotechnol.* **2014**, *9*, 193–197.
- C. I. Richards, S. Choi, J.-C. Hsiang, Y. Antoku, T. Vosch, A. Bongiorno, Y.-L. Tzeng, R.M. Dickson, *J. Am. Chem. Soc.* **2008**, *130*, 5038–5039.
- W. Guo, J. Yuan, Q. Dong, E. Wang, *J. Am. Chem. Soc.* **2010**, *132*, 932–934.
- I. Díez, R. H. A. Ras, *Nanoscale* **2011**, *3*, 1963–1970.
- L. A. Gugliotti, D. L. Feldheim, B. E. Eaton, *Science*. **2004**, *304*, 850–852.
- L. A. Gugliotti, D. L. Feldheim, B.E. Eaton, *J. Am. Chem. Soc.* **2005**, *127*, 17814–17818.
- R. R. Naik, S. Jones, C. Murray, J. McAuliffe, R. Vaia, M. O. Stone, *Adv. Funct. Mater.* **2004**, *14*, 25–30.
- R. R. Naik, S. Stringer, G. Agarwal, S. Jones, M. O. Stone, *Nature Materials.* **2002**, *1*, 169–172.
- S. Whaley, D. English, E. Hu, P. Barbara, A. Belcher, *Nature*. **2000**, *405*, 665–668.
- J. M. Slocik, M. O. Stone, R.R Naik, *Small*. **2005**, *1*, 1048–1052.
- S. Diamanti, A. Elsen, R. R. Naik, R. Vaia, *J. Phys. Chem. C.* **2009**, *113*, 9993–9997.
- J. Yu, M. L. Becker, G. A. Carri, *Langmuir*. **2012**, *28*, 1408–1417.

- 29 M. M. Tomczak, J. M. Slocik, M. O. Stone, R. R. Naik, *Biochem. Soc. Trans.* **2007**, *35*, 512–515.
- 30 C.-L. Chen, P. Zhang, N. L. Rosi, *J. Am. Chem. Soc.* **2008**, *130*, 13555–13557.
- 31 C.-L. Chen, N. L. Rosi, *Angew. Chem. Int. Ed.* **2010**, *49*, 1924–1942; *Angew. Chem.* **2010**, *122*, 1968–1986
- 32 J. N. Cha, K. Shimizu, Y. Zhou, S. C. Christiansen, B. F. Chmelka, G. D. Stucky, D. E. Morse, *Proc. Natl. Acad. Sci. U.S.A.* **1999**, *96*, 361–365.
- 33 P. Curnow, P. H. Bessette, D. Kisailus, M. M. Murr, P. S. Daugherty, D. E. Morse, *J. Am. Chem. Soc.* **2005**, *127*, 15749–15755.
- 34 G. P. Smith, K. J. Baustian, C. J. Ackerson, D. L. Feldheim, *J. Mater. Chem.* **2009**, *19*, 8299–8306.
- 35 D. Scott, M. Toney, M. Muzikár, *J. Am. Chem. Soc.* **2008**, *130*, 865–874.
- 36 S. Silver, L. T. Phung, *J. Ind. Microbiol. Biotechnol.* **2005**, *32*, 587–605.
- 37 M. Lenz, B. Kolvenbach, B. Gyax, S. Moes, P. F. X. Corvini, *Appl. Environ. Microbiol.* **2011**, *77*, 4676–4680.
- 38 W. J. Hunter, *Curr. Microbiol.* **2014**, *69*, 69–74.
- 39 J. Kessi, *Microbiology.* **2006**, *152*, 731–743.
- 40 M. Bozzi, G. Mignogna, S. Stefanini, D. Barra, C. Longhi, P. Valenti, E. Chiancone, *J. Biol. Chem.* **1997**, *272*, 3259–3265.
- 41 N. Kroger, M. B. Dickerson, G. Ahmad, Y. Cai, M. S. Haluska, K. H. Sandhage, N. Poulsen, V. C. Sheppard, *Angew. Chem. Int. Ed.* **2006**, *45*, 7239–7243; *Angew. Chem.* **2006**, *118*, 7397–7401
- 42 U. Tinggi, *Toxicol. Lett.* **2003**, *137*, 103–110.
- 43 W. J. Hunter, D. K. Manter, *Curr. Microbiol.* **2008**, *57*, 83–88.
- 44 W. J. Hunter, D. K. Manter, *Curr. Microbiol.* **2009**, *58*, 493–498.
- 45 R. S. Oremland, M. J. Herbel, J. S. Blum, S. Langley, T. J. Beveridge, P. M. Ajayan, T. Sutto, A. V. Ellis, S. Curran, *Appl. Environ. Microbiol.* **2004**, *70*, 52–60.
- 46 M. S. Galeas, L. H. Zhang, J. L. Freeman, M. Wegner, E. A. H. Pilon-Smits, *New Phytologist.* **2006**, *173*, 517–525.
- 47 W. J. Hunter, D. K. Manter, *Curr. Microbiol.* **2011**, *62*, 565–569.
- 48 R. McIntosh, D. Nicastro, D. Mastronarde, *Trends Cell. Biol.* **2005**, *15*, 43–51.
- 49 C. V. Robinson, A. Sali, W. Baumeister, *Nature* **2007**, *450*, 973–982.
- 50 K. McDonald, M. K. Morphew, *Microsc. Res. Tech.* **1993**, *24*, 465–473.
- 51 T. H. Giddings, *Journal of Microscopy* **2003**, *212*, 53–61.
- 52 C. V. Iancu, W. F. Tivol, J. B. Schooler, D. P. Dias, G. P. Henderson, G. E. Murphy, E. R. Wright, Z. Li, Z. Yu, A. Briegel, L. Gan, Y. He, G. J. Jensen, *Nature Protocols* **2006**, *1*, 2813–2819.
- 53 A. S. Frangakis, J. Böhm, F. Förster, S. Nickell, D. Nicastro, D. Typke, R. Hegerl, W. Baumeister, *Proc. Natl. Acad. Sci. USA* **2002**, *99*, 14153–14158.
- 54 S. Nickell, C. Kofler, A. P. Leis, W. A. Baumeister, *Nat. Rev. Mol. Cell. Biol.* **2006**, *7*, 225–230.
- 55 A. Komeili, Z. Li, D. Newman, G. J. Jensen, *Science* **2006**, *311*, 242–245.
- 56 G. J. Jensen, A. Briegel, *Curr. Opin. Struct. Biol.* **2007**, *17*, 260–267.
- 57 C. S. Butler, C. M. Debieux, E. J. Dridge, P. Splatt, M. Wright, *Biochem. Soc. Trans.* **2012**, *40*, 1239–1243.
- 58 M. Basaglia, A. Toffanin, E. Baldan, M. Bottegai, J. P. Shapleigh, S. Casella, *FEMS Microbiol. Lett.* **2007**, *269*, 124–130.
- 59 C. Garbisu, T. Ishii, T. Leighton, B. B. Buchanan, *Chem. Geol.* **1996**.
- 60 M. B. Jornstedt, S. Kumar, A. Holmgren, *Meth. Enzymol.* **1995**.
- 61 J. Lu, Y. Xie, F. Xu, L. Zhu, *J. Mater. Chem.*, **2002**, *12*, 2755–2761
- 62 W. Margolin, *J. Bacteriol* **2012**, *194*, 6369–6371.
- 63 M. T. Swulius, G. J. Jensen, *J. Bacteriol.* **2012**, *194*, 6382–6386.
- 64 J. D. Corbett, *Chem Rev* **1985**, *85*, 383–397.
- 65 T. Scopigno, W. Steurer, S. N. Yannopoulos, A. Chrissanthopoulos, M. Krisch, G. Ruocco, T. Wagner, *Nat. Commun.* **2011**, *2*, 195.
- 66 S. Kumar, M. Björnstedt, A. Holmgren, *Eur. J. Biochem.* **1992**, *207*, 435–439.
- 67 C. J. Ackerson, R. D. Powell, J. F. Hainfeld, *Meth. Enzymol.* **2010**, *481*, 195–230.
- 68 M. Björnstedt, S. Kumar, A. Holmgren, *J. Biol. Chem.* **1992**, *267*, 8030–8034.